DFT Study of the Asymmetric Nitroaldol (Henry) Reaction Catalyzed by a Dinuclear Zn Complex

NA QI, RONG-ZHEN LIAO, JIAN-GUO YU, RUO-ZHUANG LIU
College of Chemistry, Beijing Normal University, Beijing 100875, China

Received 19 March 2009; Revised 22 July 2009; Accepted 20 August 2009
DOI 10.1002/jcc.21422
Published online 17 December 2009 in Wiley InterScience (www.interscience.wiley.com).

Abstract: We report the mechanism of asymmetric nitroaldol (Henry) reaction catalyzed by a dinuclear Zn complex using density functional theory. The experimentally proposed catalytic cycle is validated, in which the first step is the deprotonation of nitromethane by the ethyl anion of the catalyst, subsequently a C—C bond formation step, and then the protonation of the resulting alkoxide. Three mechanistic scenarios (differing in binding modes) have been considered for the C—C bond formation step. The origin of the enantioselectivity is discussed. Our calculations supported that the S configurations are the major products, which is in agreement with the experimental observations.

 J Comput Chem 31: 1376–1384, 2010

Key words: nitroaldol (Henry) reaction; density functional theory; enantioselectivity; dinuclear Zn catalyst

Introduction

The Henry or nitroaldol reaction, between carbonyl compounds and nitroalkanes, constitutes a very important synthetic method for the construction of carbon–carbon bonds in organic chemistry.[1] The resulting β-nitroaldols, especially in an optically active form, are useful precursors to a variety of valuable functionalized structural motifs, such as β-amino alcohols, α-hydroxy carboxylic acids, etc. These derivatives are common building blocks presented in biologically active nature products and pharmaceuticals.[2] Consequently, considerable efforts have been made toward the development of efficient asymmetric catalysts for this kind of reactions with impressive breakthrough achieved over the last two decades.[3,4]

With the presence of a number of environmentally friendly organocatalysts for the nitroaldol reaction, many bifunctional metal/chiral ligand complexes have also been described with high efficiency, including lanthanoid,[5–7] Zn,[8–11] Cu,[12–15] and Co[16,17] complexes. Apparently, zinc-based catalysts are especially interesting because they parallel class II aldolase enzymes in the light of relying on zinc.[18] Several efficient mononuclear zinc catalysts with different chiral ligands have been developed for this reaction, such as chiral amino alcohol,[9] bisoxazolidine,[10] and ferrocenyl-substituted aziridinylmethanol.[11] In addition, some other mononuclear Zn-based catalysts have also been reported, however, with lower enantiomeric excesses.[19] Beside these mononuclear zinc catalysts, Trost and Yeh[8] reported the first asymmetric dinuclear zinc complexes **1** with a chiral semi-azacrown ligands (see Scheme 1), which were found to be efficient catalysts for inducing unparalleled enantioselectivity.

The dinuclear zinc catalyst designed by Trost also led to a number of other efficient, catalytic, enantioselective transformations, including aldol reactions,[20–24] Mannich reactions,[25,26] Michael addition,[27] alkynylations of aldehydes,[28] desymmetrizations of *meso* 1,3-diols,[29] and Friedel-Crafts alkylations.[30] The catalyst has also been successfully applied in natural product synthesis and other important chemical reactions.[31–34] For nitroaldol reactions, Trost proposed a possible catalytic cycle, as depicted in Scheme 2. The initial step of the reaction is deprotonation of nitromethane by the ethyl anion attached to one of the zinc ions in the catalyst, resulting in the formation of a zinc nitronate intermediate and 1 equiv of ethane. Coordinations of the aldehyde to the other zinc ion undergo the C—C bond formation between the nitronate carbon and the aldehyde carbon. Finally, the association of nitromethane followed by a proton transfer to the oxygen anion produced in the previous step gives the product and restart the catalytic cycle.[8]

A number of zinc-catalyzed reactions have been investigated by means of quantum chemical methods.[35–39] However, accord-

Additional Supporting Information may be found in the online version of this article.

The first two authors contributed equally to this paper.

Correspondence to: J-G. Yu; e-mail: jianguo_yu@bnu.edu.cn

Contract/grant sponsor: National Natural Science Foundation of China; contract/grant numbers: 20733002, 20873008

Contract/grant sponsor: Major State Basic Research Development Programs; contract/grant number: 2004CB719903

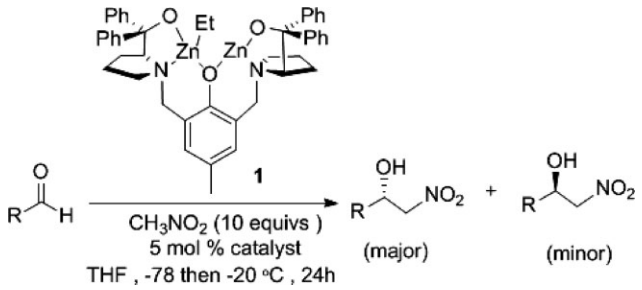

Scheme 1. Catalyzed asymmetric Henry reaction.

ing to our knowledge, little theoretical attention has been paid for this dinuclear zinc catalyst. Despite the great achievements in the experimental area on the study of the reaction, insight into the energetic, the detailed mechanism and the origin of the enantioselectivity of this catalytic reaction are still lacking. These have prompted our theoretical investigation for the mechanism of the reaction catalyzed by this binuclear Zn catalyst. In our present study, we performed the density functional calculations with the well-established B3LYP functional,[40,41] and chose the benzaldehyde and nitromethane as substrates, yielding 2-nitro-1-phenylethanol (see Scheme 3). Our calculations are relevant to further understanding of many other reactions catalyzed by this dinuclear Zn catalyst.

Computational Details

All calculations were performed at the density functional theory (DFT) level with the B3LYP functional as implemented in the Gaussian 03 package.[42] For the geometry optimizations, the 6-31G(*d,p*) basis sets were used for the C, N, O, and H elements and the SDD pseudopotential[43] for Zn. Based on the optimized geometries, more accurate energies were obtained by performing single-point calculations with the 6-311++G(*2d,2p*) basis sets for all elements. All geometries were optimized *in vacuo*. To estimate the energetic effects of the THF ($\varepsilon = 7.58$) environment, solvation effects were calculated at the same theory level as the optimizations by performing single-point calculations on the optimized structures using the conductor-like polarizable continuum model (CPCM) method.[44–47] Frequency calculations were performed at the same theory level as the optimizations to obtain zero-point energies (ZPE) and to confirm the nature of all stationary points. The latter implied no negative eigenvalues for minima and only one negative eigenvalue for transition states. The energies reported herein were corrected for both solvation and zero-point vibrational effects.

To compare the results obtained with the B3LYP method, we also used a new hybrid density functional BB1K that has recently been shown to produce results for accurate potential energy surface (PES) calculation of reactions.[48] Based on the optimized geometries with B3LYP for some important configurations, we carried out single-point calculations by BB1K, and the 6-31G(*d,p*) basis sets were used for the C, N, O, and H elements and the SDD pseudopotential for Zn. Additionally, single-point calculations with the 6-311++G(*2d,2p*) basis sets for all elements were also carried out to get more accurate energies. All results have been corrected for both solvation in THF and zero-point vibrational effects.

Results and Discussion

Based on our calculations, it was found that the catalytic reaction involves three chemical steps: (1) deprotonation of nitrome-

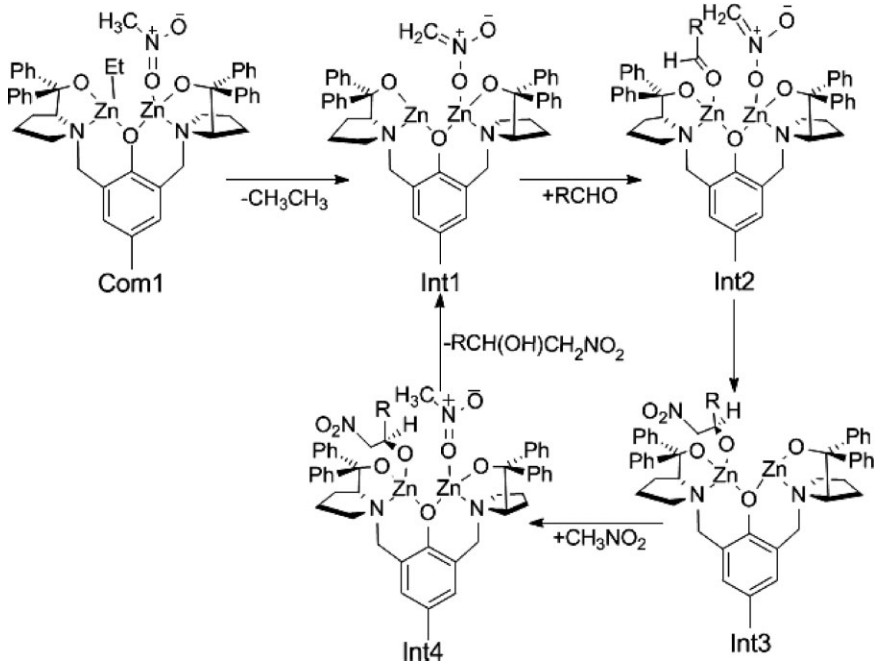

Scheme 2. Proposed catalytic cycle for the Henry reaction.[8]

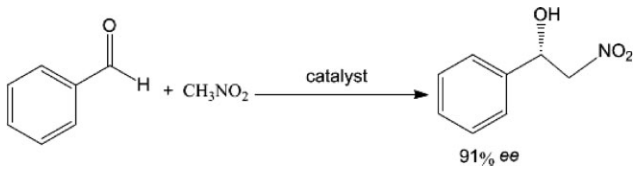

Scheme 3. The Henry reaction between benzaldehyde and nitromethane discussed in this paper.

thane, (2) C—C bond formation, and (3) proton transfer and regeneration of the reactive species.

Step 1: Deprotonation

The first step is the deprotonation of nitromethane by the ethyl anion coordinated to Zn1 in Com1 ($Com1_A$ and $Com1_B$, see Supporting Information) with the formation of Int1 and ethane. Because of the coordination of nitromethane to Zn2, the energy of $Com1_A$ is 9.7 kcal/mol lower than that of isolated reactants in the gas phase and 5.7 kcal/mol in the THF. Two plausible mechanistic pathways have been considered, one is with the retention of the carbon configuration, marked as I_A, whereas the second is with the inversion of the carbon configuration, marked as I_B. The corresponding transition states are labeled as $TS1_A$ and $TS1_B$ (Fig. 1) with the barriers to be 20.6 (22.6) kcal/mol (energies in parenthesis correspond to calculations in gas phase) relative to $Com1_A$ and 20.4 (22.3) kcal/mol relative to $Com1_B$ including THF solvation effect (Fig. 2), respectively. However, $TS1_A$ is 1.8 kcal/mol (4.4 kcal/mol by the BB1K method) lower than $TS1_B$. These results indicate that the retention pathway is more favorable. At $TS1_A$, the two C—H distances are 1.349 and 1.484 Å, respectively, and the angle between C—H—C is 164.2°; whereas at $TS1_B$, the two C—H distances are 1.395 Å and 1.487 Å, and the angle is 154.9°; (Fig. 1).

This step is exothermic by over 30 kcal/mol from our calculations (Fig. 2), indicating that the proton transfer is energetically quite feasible. The reason may be the large difference of the relative pKa between nitromethane and ethane.

Step 2: Carbon–Carbon Bond Formation

With the formation of a reactive nitronate species in **Int1**, the benzaldehyde can easily undergo a nucleophilic attack with the formation of C—C bond. Three plausible binding modes of the nucleophile to Zn2 have been considered, which are marked as pathways A, B, C. The fragment structures of the reactants (**Int2**) leading to S-products and R-products are shown in Figure 3.

In pathway A, the nitronate is coordinated to the dinuclear zinc center in a bidentate fashion (Fig. 3), with the Zn1-O and Zn2-O distances of 2.131 and 1.975 Å in $Int2_{SA}$, 2.117 and 1.967 Å in $Int2_{RA}$, respectively. The structures of the transition states ($TS2_{SA}$ and $TS2_{RA}$ in Fig. 4) that lead to both S and R products have been located. $TS2_{SA}$ is 9.1 (9.8) kcal/mol higher in energy than $Int2_{SA}$, whereas $TS2_{RA}$ is 13.3(12.2) kcal/mol higher than $Int2_{RA}$. The C—C distances in $TS2_{SA}$ and $TS2_{RA}$ are 2.143 and 2.011 Å, respectively. In addition, the corresponding dihedral angles of O31-C30-C29-N27 in both transition states (Fig. 4) are 27.2° and −9.3°, respectively. Downhill from the transition states, the nitroalkoxide catalyst complex (**Int3**, see **SI**) is formed, and the energies of $Int3_{SA}$ and $Int3_{RA}$ are 5.4 and 4.3 kcal/mol relative to $Int2_{SA}$ and $Int2_{RA}$, respectively. During the step of C—C bond formation, the negative charge is transferred from the nitronate oxygen to benzaldehyde oxygen. In $Int3_{SA}$, the newly formed oxyanion is stabilized by Zn1 with the corresponding distance of 1.910 Å. But the oxyanion is coordinated to both Zn ions in $Int3_{RA}$, with the Zn1-O31 and Zn2-O31 distances of 1.968 and 2.052 Å, respectively. Both Zn ions provide electrostatic stabilization on both the transition states and intermediates, thereby lowering the barrier for the C—C bond formation.

In pathway B, the nitronate is coordinated to Zn2 with both oxygen atoms (Fig. 3). The calculated Zn—O distances are 2.194 and 2.098 Å in $Int2_{SB}$, and 2.195 and 2.094 Å in $Int2_{RB}$, respectively. The barriers for the C—C bond formation starting from these structures are 6.3 (5.1) kcal/mol for the S-product ($Int3_{SB}$) and 9.0 (6.6) kcal/mol for the R-product ($Int3_{RB}$). The key C—C distances are 2.132 Å and 2.053 Å in $TS2_{SB}$ and $TS2_{RB}$ (Fig. 4), respectively. Additionally, the dihedral angles of O31-C30-C29-N27 in $TS2_{SB}$ and $TS2_{RB}$ are 40.5° and 34.7°, respectively. The energy of the $Int3_{SB}$ lies at −4.2 kcal/mol relative to $Int2_{SB}$, whereas that of $Int3_{RB}$ is 8.6 kcal/mol higher than $Int2_{RB}$. It can be seen from Figure 5 that the formation of R-product through pathway B is not favorable since the barrier for the reverse step is just 0.4 kcal/mol. The transfer of $Int3_{RB}$ to $Int3_{RC}$ or $Int3_{RA}$ should require at least several kcal/mol, indicating that the formation of R-product through pathway B is not competitive with pathway A, although $TS2_{RB}$ is only 0.2 kcal/mol lower than $TS2_{RA}$.

Based on our calculations, in pathway C, an oxygen atom of the nitronate is coordinated to both Zn ions (Fig. 3), with the Zn1-O and Zn2-O distances of 2.163 and 1.990 Å in $Int2_{SC}$, 2.132 and 1.987 Å in $Int2_{RC}$. The transition states of C—C bond formation from $Int2_{SC}$ and $Int2_{RC}$ ($TS2_{SC}$ and $TS2_{RC}$, see Fig. 4) are located with the C—C bond distance of 2.255 and 2.258 Å, with the energetic barriers of 7.3 (7.2) and 4.5 (5.2) kcal/mol, respectively. Furthermore, the dihedral angle of O31-C30-C29-N27 in the TS structures was calculated as 69.1° and 63.3°. The reaction of this pathway for the formation of S and R products ($Int3_{SC}$ and $Int3_{RC}$) is exothermic by 7.2 and 7.7 kcal/mol, respectively. In both $Int3_{SC}$ and $Int3_{RC}$, the nitroalkoxide oxygen anion is bridging the two Zn ions (see **SI**).

In the three pathways discussed above, according to their relative reaction barriers, the pathway A is energetically the most favorable (see Fig. 5), whereas the pathway B is next. There could be a couple of reasons. One reason for the order could be that the $Int2_{SA}$ and $Int2_{RA}$ adopt an energetically more feasible conformation, evidenced by the relative energies of six reactants in this step (see Fig. 5). Another reason might be the stronger interactions between Zn1 and n electrons of O31. At TS2, O31 changes from *sp2* hybridization in Int2 to partially *sp3* hybridization. The angle of C30-O31-Zn1 (labeled as α in Fig. 4) is 123.0° in $TS2_{SA}$. However, the angles are 129.4° in $TS2_{SB}$ and 135.7° in $TS2_{SC}$.

The overall reaction between nitromethide and benzaldehyde yielding nitroalkoxide (Re, TS, and Pr in **SI**) was calculated to

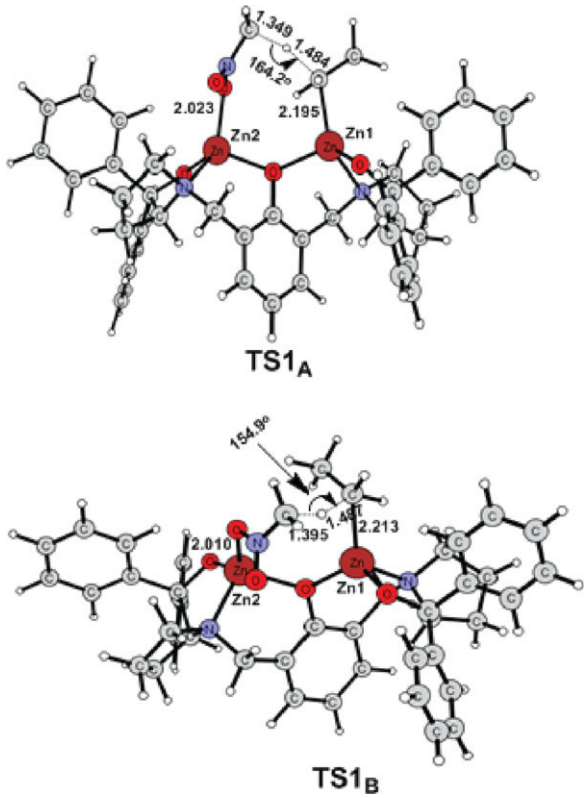

Figure 1. Optimized structures of the transition states for the proton transfer from nitromethane to the ethyl anion in two pathways (distances in Å).

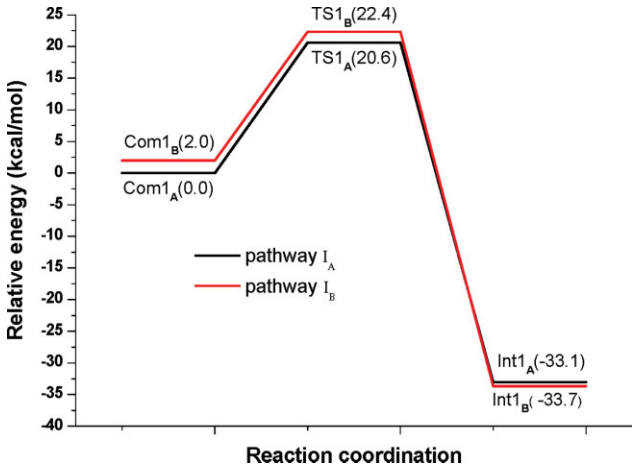

Figure 2. Calculated relative energetic (kcal/mol) profile (including solvation) for the deprotonation step.

be endothermic by 7.3 (7.7) kcal/mol, indicating that the dinuclear zinc center provides more stabilization on the unprotonated product by as much as 8.3 kcal/mol in THF. However, the barrier for the catalytic C—C bond formation does not change much compared with uncatalyzed one [8.6 (8.4) kcal/mol]. Our results are different from previous calculations on reaction between nitromethide and formaldehyde.[49] The recent results show that the barrier and the reaction energy are 3.2 and −1.4 kcal/mol at the CCSD(T)/aug-cc-pVDZ//MP2/6-31+G(d) level in gas phase.[50] The main reason is due to the stronger hydrogen

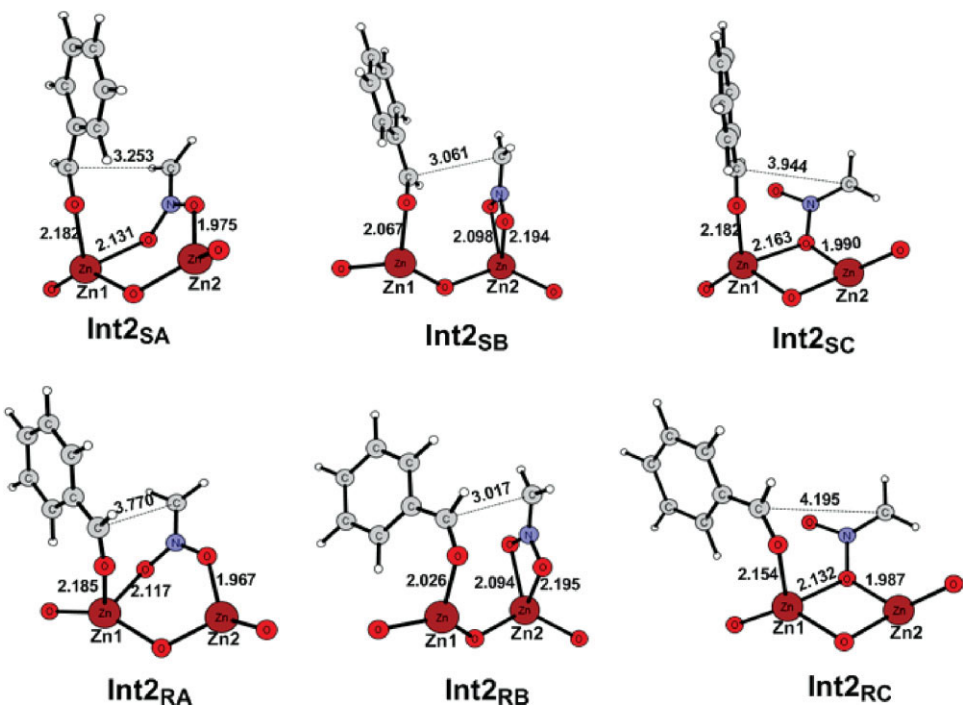

Figure 3. The six segments of the intermediates corresponding to three reaction pathways (distances in Å).

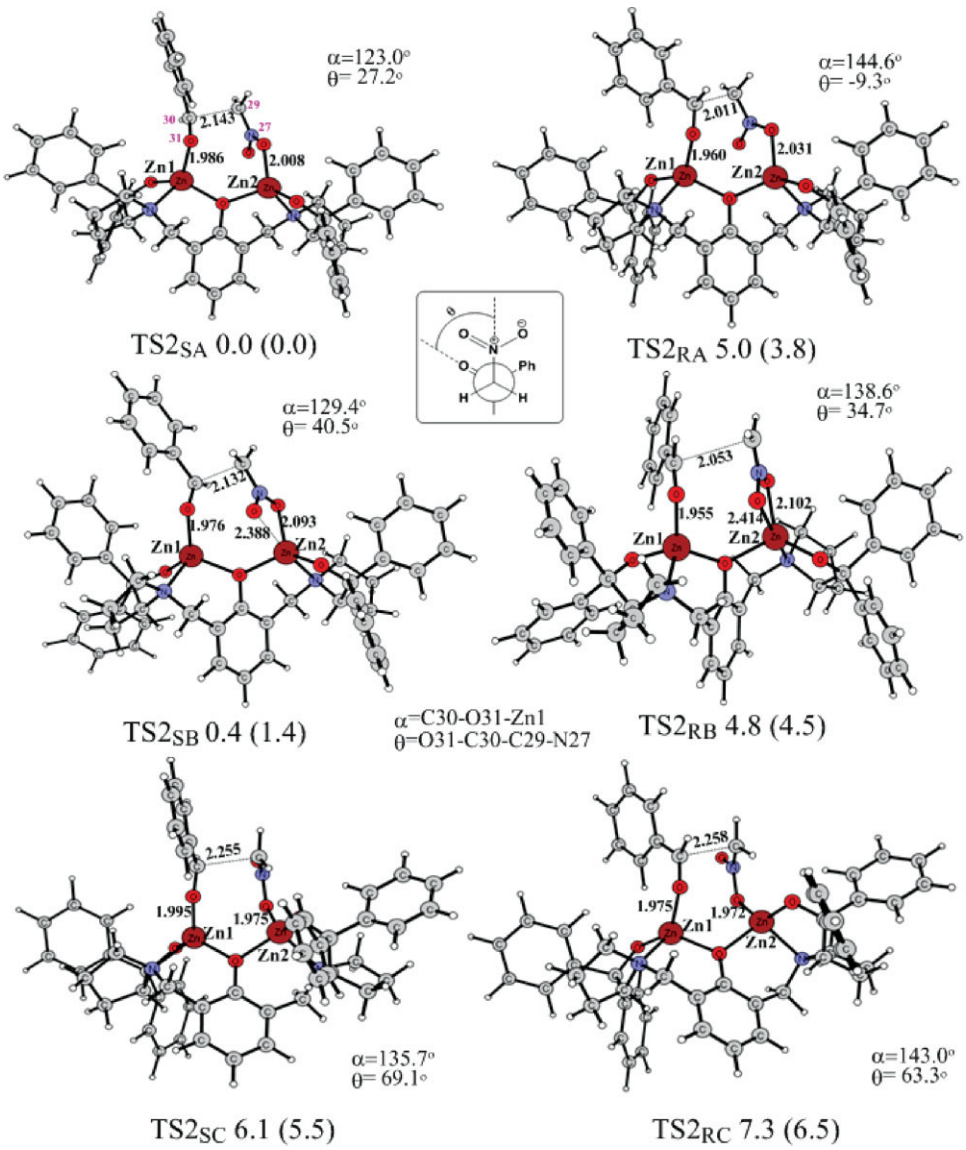

Figure 4. The geometries of optimized transition states for C—C bond formation through pathway A ($TS2_{SA}$, $TS2_{RA}$), pathway B ($TS2_{SB}$, $TS2_{RB}$) and pathway C ($TS2_{SC}$, $TS2_{RC}$). Framed insets define the dihedral angles specified. Relative energies (kcal/mol) for the six transition states including solvation correction are given in the labels (gas phase values in parentheses) (distances in Å).

bond between nitromethide and benzaldehyde comparing with that between nitromethide and formaldehyde, which stabilizes the reactant too much.

Enantioselectivity

It was found by Trost that this dinuclear Zn catalyst could catalyze many reactions with high efficiency and enantioselectivity. The reaction of benzaldehyde and nitromethane catalyzed by 5 mol% catalyst proceeds with considerable asymmetric induction (91% *ee*).[8] However, the reason for the high enantioselectivity in the reactions was not well elucidated so far. The phenyl rings of the diphenylcarbinol moiety were suggested to be involved in chiral recognition.[22]

In the present study, we have optimized the transition states leading to both enantiomers for all three pathways. We first note that the TS with the lowest energy ($TS2_{SA}$) corresponds to S-product, in agreement with the experimental findings that the major enantiomer of nitroaldol is S-configuration.[8] The energy difference between $TS2_{SA}$ and $TS2_{RA}$ is 5.0 (3.8) kcal/mol, which has a gap with the experimentally observed ee of 91%. However, with BB1K functional, the energy difference is 1.8 kcal/mol in THF. So the method may have deviations, but all these results suggested that our results are consistent with the experimental trend.

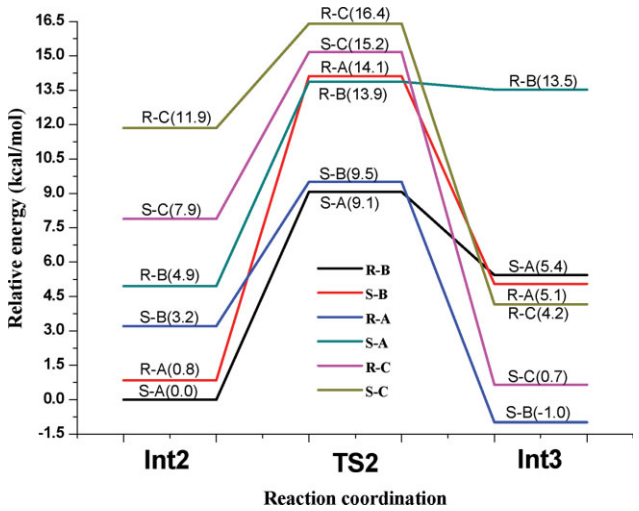

Figure 5. Calculated relative energetic (kcal/mol) profile for C—C bond formation (including solvation). [Color figure can be viewed in the online issue, which is available at www.interscience.wiley.com.]

Table 1. Summary of the Calculated Relative Energies (kcal/mol) for the C—C bond Formation Step Through Preferred Pathway A, for Catalyst with Four Phenyl Groups, or Four Methyl Groups and Four Hydrogen Atoms.

	Phenyl—	CH_3—	H—
$Int2_{SA}$	0.0 (0.0)	0.0 (0.0)	0.0 (0.0)
$TS2_{SA}$	9.1 (9.8)	11.0 (8.6)	11.1 (9.7)
$Int3_{SA}$	5.4 (6.0)	7.4 (4.7)	7.2 (5.6)
$Int2_{RA}$	0.8 (1.4)	2.7 (0.8)	0.4 (−0.3)
$TS2_{RA}$	14.1 (13.6)	14.5 (11.4)	13.3 (11.1)
$Int3_{RA}$	5.1 (2.2)	6.6 (1.0)	3.3 (−0.6)

We noticed that the Mulliken charge of C29 and C30 in $Int2_{SA}$ is −0.143 and +0.236 e, respectively; whereas it is −0.125 and +0.223 e in $Int2_{RA}$. The stronger electrostatic interaction between C29 and C30 may result in lower barrier for the C—C bond formation. In addition, we noted that the α angles (C30-O31-Zn1) in TS2 with S configurations are all smaller than those with R configurations (see Fig. 4). The reason should be

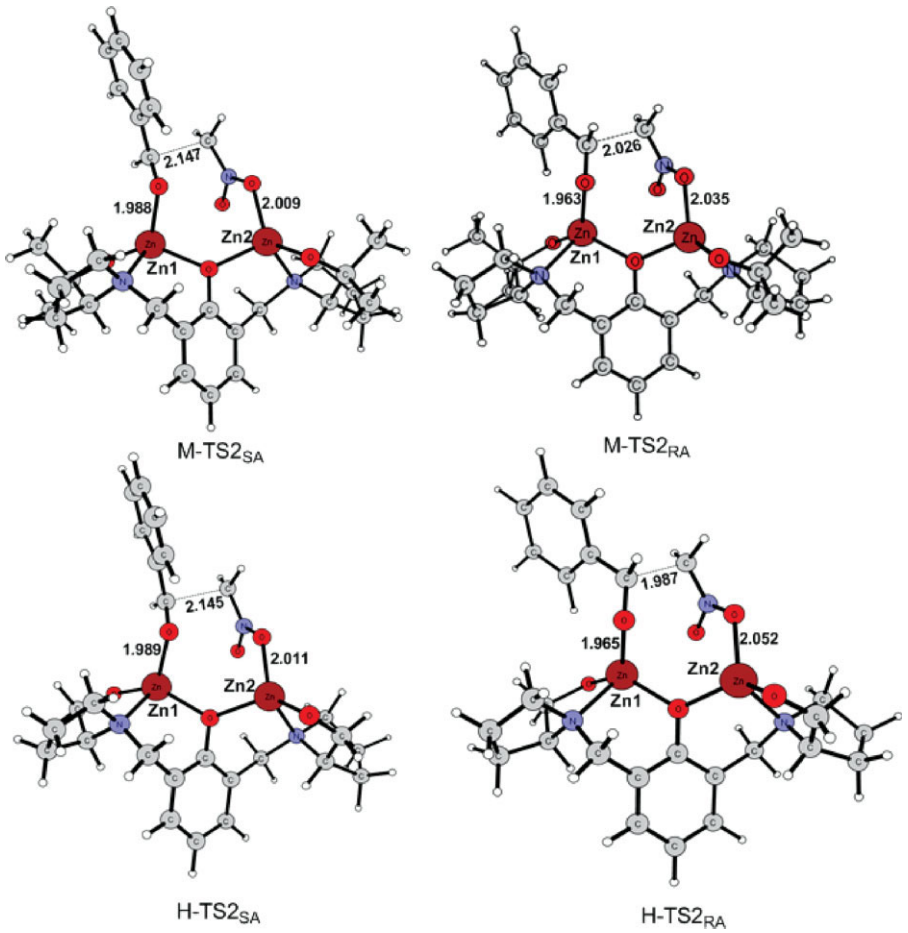

Figure 6. The structures of the transition states for S and R products through more favored pathway A with phenyl groups substituted by methyl groups and hydrogen atoms (Distances in Å). [Color figure can be viewed in the online issue, which is available at www.interscience.wiley.com.]

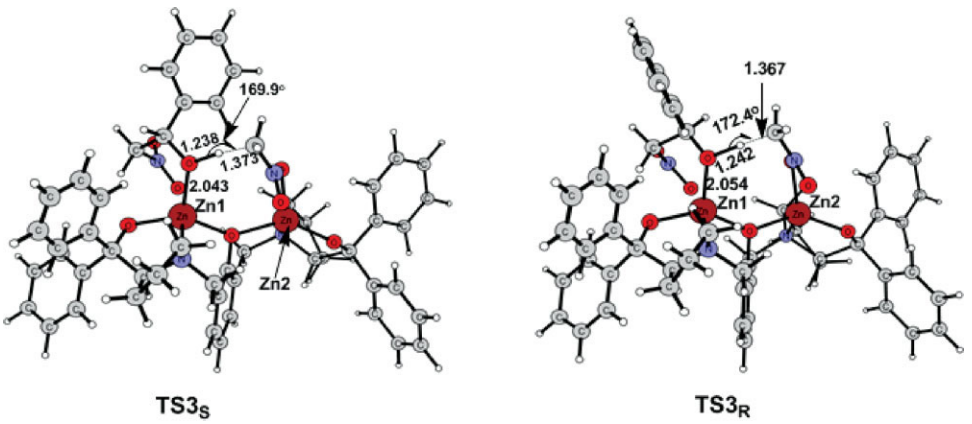

Figure 7. Optimized structures of the two transition states for the proton transfer from nitromethane to the nitroalkoxide oxygen anion (Distances in Å). [Color figure can be viewed in the online issue, which is available at www.interscience.wiley.com.]

the steric repulsions between the phenyl ring of benzaldehyde and the carbinol oxygen coordinated to Zn1.

To clarify the role of the four phenyl rings in the catalyst, we have optimized the structures of the catalyst with phenyl groups replaced by methyl groups and hydrogen atoms. The structures of transition states (M-TS2$_{SA}$, M-TS2$_{RA}$, and H-TS2$_{SA}$, H-TS2$_{RA}$) are shown in Fig. 6, whereas the structures of all intermediates are depicted in **SI**. As expected, the overall geometries are quite similar to the ones with phenyl groups discussed above. However, the energy difference for the two TS leading to S and R products becomes 3.5 (2.8) kcal/mol for CH_3-substituted catalyst, and 2.2 (1.4) kcal/mol for H-substituted catalyst (see Table 1). Comparing with the energy difference of 5.0 (3.8) kcal/mol in the phenyl-substituted catalyst, these results suggest that the larger the substitutes are, the better the enantioselectivity for this reaction is. That is to say, the phenyl rings play a key role in governing the enantioselectivity for this asymmetric reaction.

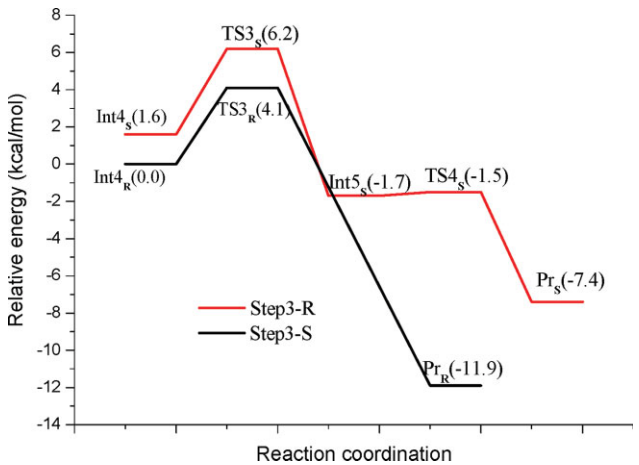

Figure 8. Calculated potential energy (kcal/mol) profile (including solvation) for step 3. [Color figure can be viewed in the online issue, which is available at www.interscience.wiley.com.]

Step 3: Proton Transfer

Trost and Yeh[8] proposed that formation of C—C bond would result in a nitroalkoxide, which can undergo protonation by a new nitromethane coordinated to Zn2. Such a proton transfer can generate a new reactive nitronate, and restart the catalytic cycle.

We found from our calculations that on the coordination of the other nitromethane, the S-complex (Int4$_S$) is 1.6 kcal/mol higher than R-complex (Int4$_R$). The optimized transition states for the proton transfer (TS3$_S$ and TS3$_R$) are shown in Figure 7. The barriers of the reactions are 4.6 (5.2) kcal/mol and 4.1 (5.1) kcal/mol relative to Int4$_S$ and Int4$_R$, respectively (Fig. 8). In the TS3$_S$, the transferred proton is sandwiched between the nitroalkoxide oxygen and the nitromethane carbon, with the O—H and C—H distance of 1.238 Å and 1.373 Å, respectively. The main part of the TS3$_R$ geometry is quite similar to that of TS3$_S$, with the corresponding O—H and C—H distance of 1.242 Å and 1.367 Å, respectively. At the end, the products complexed with the catalyst (Pr$_S$ and Pr$_R$, see **SI**) are formed, with a hydrogen bond between the nitronate oxygen and 2-nitro-1-phenylethanol. It was noted that an additional intermediate Int5$_S$ (see **SI**) lies between TS3$_S$ and Pr$_S$, with a hydrogen bond between the nitronate carbon and 2-nitro-1-phenylethanol. From Int5$_S$ to Pr$_S$, we find a new transition state which is named as TS4 (see **SI**). It corresponds to the formation of a new hydrogen bond. The energy barrier is only 0.2 kcal/mol (Fig. 8), which suggests that the transformation is very fast.

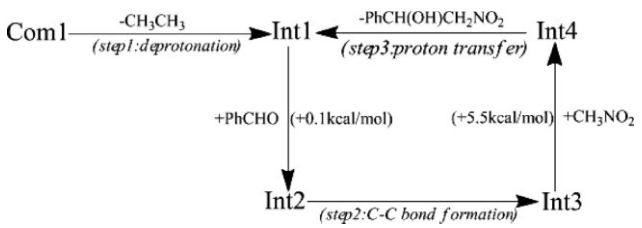

Scheme 4. Calculated catalytic cycle for the Henry reaction.

Because the catalytic cycle contains just step 2 and step 3, our calculations suggest that step 2 determines the reaction kinetics, which is consistent with experimental results for the main product is S-configuration.

Conclusions

In the present paper, we have investigated the reaction mechanism and the enantioselectivity of the reaction of benzaldehyde and nitromethane catalyzed by the dinuclear zinc complex **1**. The potential-energy profiles were calculated by means of DFT methods. Our calculations strongly support the experimentally proposed catalytic cycle as shown in Scheme 2 (See Scheme 4 for the calculating steps and energetics of some steps and involved species). The detailed mechanisms for all three steps are discussed, especially the enantioselectivity determining C—C bond formation step.

For step 1, two plausible proton transfer channels involving the retention (I_A) and the inversion (I_B) of the configuration have been considered, with I_A slightly preferred. For the C—C bond formation step, three possible pathways (pathways A, B, C) have been found. Pathway A is energetically preferred over other two pathways. Both zinc ions are involved in stabilizing the negative charge in the transition states and intermediates. The enantioselectivity mainly comes from the steric repulsion between the benzaldehyde and the phenyls of the catalyst. The preferred S-product is in agreement with the experimental findings. In the following step, the proton transfer between the nitroalkoxide and a new nitromethane can generate the product nitroalcohol and a new reactive species ready for the next catalytic cycle. For the reaction cycle, the C—C bond formation step is rate limiting.

We can speculate that this dinuclear zinc complex may catalyze other transformations[20–24] through similar mechanistic issues. Theoretical studies of other catalytic C—C bond formation reactions are in progress.

Acknowledgments

We thank Dr. Sven de Marothy (of Stockholm University) for providing xyz viewer to draw all the figures of the molecule models.

References

1. Henry, L. Acad Sci Ser C 1895, 120, 1265.
2. Luzzio, F. A. Tetrahedron 2001, 57, 915.
3. Boruwa, J.; Gogoi, N.; Saikia, P. P.; Barua, N. C. Tetrahedron: Asymmetry 2006, 17, 3315.
4. Palomo, C.; Oiarbide, M.; Laso, A. Eur J Org Chem 2007, 16, 2561.
5. Sasai, H.; Suzuki, T.; Arai, S.; Arai, T.; Shibasaki, M. J Am Chem Soc 1992, 114, 4418.
6. Arai, T.; Yamada, Y. M. A.; Yamamoto, N.; Sasai, H.; Shibasaki, M. Chem Eur J 1996, 2, 1368.
7. Iseki, K.; Oishi, S.; Sasai, H.; Shibasaki, M. Tetrahedron Lett 1996, 37, 9081.
8. Trost, B. M.; Yeh, V. S. C. Angew Chem Int Ed 2002, 41, 861.
9. Palomo, C.; Oiarbide, M.; Laso, A. Angew Chem Int Ed 2005, 44, 3881.
10. Liu, S.; Wolf, C. Org Lett 2008, 10, 1831.
11. Bulut, A.; Aslan, A.; Dogan, Ö. J Org Chem 2008, 73, 7373.
12. Christensen, C.; Juhl, K.; Hazell, R. G.; Jørgensen, K. A. J Org Chem 2002, 67, 4875.
13. Evans, D. A.; Seidel, D.; Rueping, M.; Lam, H. W.; Shaw, J. T.; Downey, C. W. J Am Chem Soc 2003, 125, 12692.
14. Du, D.-M.; Lu, S.-F.; Fang, T.; Xu, J. J Org Chem 2005, 70, 3712.
15. Gan, C.-S.; Lai, G.-Y.; Zhang, Z.-H.; Wang, Z.-Y.; Zhou, M.-M. Tetrahedron: Asymmetry 2006, 17, 725.
16. Kogami, Y.; Nakajima, T.; Ashizawa, T.; Kezuka, S.; Ikeno, T.; Yamada, T. Chem Lett 2004, 33, 614.
17. Kogami, Y.; Nakajima, T.; Ikeno, T.; Yamada, T. Synthesis 2004, 12, 1947.
18. Machajewski, T. D.; Wong, C.-H. Angew Chem Int Ed 2000, 39, 1352.
19. Zhong, Y.-W.; Tian, P.; Lin, G.-Q. Tetrahedron: Asymmetry 2004, 15, 771.
20. Trost, B. M.; Ito, H. J Am Chem Soc 2000, 122, 12003.
21. Trost, B. M.; Ito, H.; Silcoff, E. R. J Am Chem Soc 2001, 123, 3367.
22. Trost, B. M.; Silcoff, E. R.; Ito, H. Org Lett 2001, 3, 2497.
23. Trost, B. M.; Fettes, A.; Shireman, B. T. J Am Chem Soc 2004, 126, 2660.
24. Trost, B. M.; Shin, S.; Sclafani, J. A. J Am Chem Soc 2005, 127, 8602.
25. Trost, B. M.; Terrell, L. R. J Am Chem Soc 2003, 125, 338.
26. Trost, B. M.; Jaratjaroonphong, J.; Reutrakul, V. J Am Chem Soc 2006, 128, 2778.
27. Trost, B. M.; Hitce, J. J Am Chem Soc 2009, 131, 4572.
28. Trost, B. M.; Weiss, A. H.; Wangelin, A. J.von. J Am Chem Soc 2006, 128, 8.
29. Trost, B. M.; Mino, T. J Am Chem Soc 2003, 125, 2410.
30. Trost, B. M.; Müller, C. J Am Chem Soc 2008, 130, 2438.
31. Trost, B. M.; Yeh, V. S. C. Org Lett 2002, 4, 3513.
32. Trost, B. M.; Yeh, V. S. C.; Ito, H.; Bremeyer, N. Org Lett 2002, 4, 2621.
33. Trost, B. M.; Frederiksen, M. U.; Papillon, J. P. N.; Harrington, P. E.; Shin, S.; Shireman, B. T. J Am Chem Soc 2005, 127, 3666.
34. Trost, B. M.; Weiss, A. H. Org Lett 2006, 8, 4461.
35. Vàzquez, J.; Peric'S, M. A.; Maseras, F.; Lledós, A. J Org Chem 2000, 65, 7303.
36. Rudolph, J.; Bolm, C.; Norrby, P. O. J Am Chem Soc 2005, 127, 1548.
37. Meng, Q.-X.; Li, M.; Zhang, J.-S. J Mol Model 2006, 12, 294.
38. Wang, F.; Wang, J.-M.; Li, M. Struct Chem 2009, 20, 129.
39. Yamakawa, M.; Yamakawa, R. Organometallics 1999, 18, 128.
40. Becke, A. D. J Chem Phys 1993, 98, 5648.
41. Lee, C.; Yang, W.; Parr, R. G. Phys Rev B 1988, 37, 785.
42. Frisch, M. J.; Trucks, G. W.; Schlegel, H. B.; Scuseria, G. E.; Robb, M. A.; Cheeseman, J. R.; Montgomery, J. A.; Vreven, T, Jr.; Kudin, K. N.; Burant, J. C.; Millam, J. M.; Iyengar, S. S.; Tomasi, J.; Barone, V.; Mennucci, B.; Cossi, M.; Scalmani, G.; Rega, N.; Petersson, G. A.; Nakatsuji, H.; Hada, M.; Ehara, M.; Toyota, K.; Fukuda, R.; Hasegawa, J.; Ishida, M.; Nakajima, T.; Honda, Y.; Kitao, O.; Nakai, H.; Klene, M.; Li, X.; Knox, J. E.; Hratchian, H. P.; Cross, J. B.; Adamo, C.; Jaramillo, J.; Gomperts, R.; Stratmann, R. E.; Yazyev, O.; Austin, A. J.; Cammi, R.; Pomelli, C.; Ochterski, J. W.; Ayala, P. Y.; Morokuma, K.; Voth, G. A.; Salvador, P.; Dannenberg, J. J.; Zakrzewski, V. G.; Dapprich, S.; Daniels, A. D.; Strain, M. C.;

Farkas, O.; Malick, D. K.; Rabuck, A. D.; Raghavachari, K.; Foresman, J. B.; Ortiz, J. V.; Cui, Q.; Baboul, A. G.; Clifford, S.; Cioslowski, J.; Stefanov, B. B.; Liu, G.; Liashenko, A.; Piskorz, P.; Komaromi, I.; Martin, R. L.; Fox, D. J.; Keith, T.; Al-Laham, M. A.; Peng, C. Y.; Nanayakkara, A.; Challacombe, M.; Gill, P. M. W.; Johnson, B.; Chen, W.; Wong, M. W.; Gonzalez, C.; Pople, J. A. Gaussian 03, Revision D.01; Gaussian, Inc.: Pittsburgh, PA, 2004.
43. Bergner, A.; Dolg, M.; Kuechle, W.; Stoll, H.; Preuss, H. Mol Phys 1993, 80, 1431.
44. Barone, V.; Cossi, M. J Phys Chem A 1998, 102, 1995.
45. Cammi, R.; Mennucci, B.; Tomasi, J. J Phys Chem A 1999, 103, 9100.
46. Klamt, A.; Schmmrmann, G. J Chem Soc Perkin Trans 1993, 2, 799.
47. Tomasi, J.; Mennucci, B.; Cammi, R. Chem Rev 2005, 105, 2999.
48. Zhao, Y.; Lynch, B. J.; Truhlar, D. G. J Phys Chem A 2004, 108, 2715.
49. Lecea, B.; Arrieta, A.; Morao, I.; Cossío, F. P. Chem Eur J 1997, 3, 20.
50. Zorn, D.; Lin, V. S. Y.; Pruski, M.; Gordon, M. S. J Phys Chem A 2008, 112, 10635.